ATHENA: ASTRODYNAMICS TOOLBOX FOR HIGH-FIDELITY ERROR AND NAVIGATION ANALYSIS

Juan Manuel Romero Martin, Francesco Torre, Massimo Vetrisano, Massimiliano Vasile

University of Strathclyde.
Department of Mechanical & Aerospace Engineering.
Glasgow, UK

ABSTRACT

In this paper the main components and architecture of the ATHENA toolbox are illustrated along with a number of examples of applications.

ATHENA (Astrodynamics Toolbox for High-Fidelity Error and Navigation Analysis) is a toolbox for uncertainty propagation, guidance, navigation and control of single and multiple spacecraft with distributed architecture. This toolbox combines high fidelity dynamical and measurement models to advanced state estimation and error filtering techniques. ATHENA allows for the analysis of the coupled orbital and attitude dynamics during close proximity operations and docking with cooperative and non cooperative targets.

Index Terms— Guidance Navigation and Control, Filtering and State Estimation, Uncertainty Propagation, Operation Planning

1. INTRODUCTION

ATHENA (Astrodynamics Toolbox for High-Fidelity Error and Navigation Analysis) is a software toolbox developed over the years in the Aerospace Centre of Excellence of the University of Strathclyde to provide Guidance, Navigation and Control (GNC) solutions for a variety of complex mission scenarios and to experiment with new concepts in navigation, state estimation and uncertainty propagation. ATHENA provides capabilities for uncertainty propagation, guidance, navigation and control of single and multiple spacecraft with distributed architecture. Due to these features, the toolbox can be applied to a variety of applications, from autonomous navigation of formations or swarms of satellites in the proximity of an asteroid to close proximity operations and docking with cooperative and non-cooperative targets.

This paper will present an overview of the main components of the toolbox and a number of space mission applications that demonstrate the current capabilities of the software. In particular the paper will present the following mission scenarios:

- Navigating to the Moon along low-energy transfers
- Autonomous navigation of a spacecraft formation in the proximity of an asteroid
- Asteroid ephemerides improvement via satellite measurements
- Asteroid rotation and orbit control via laser ablation
- Autonomous collaborative on-orbit servicing

Section 2 will briefly describe the general architecture of ATHENA and its main components, then, different some key results for each of the mission scenarios will follow in Section 3.

2. ATHENA

ATHENA was conceived as a flexible and multi-disciplinary toolbox and is now an application as part of the Strathclyde Mechanical & Aerospace Research Toolbox (SMART) [1]. The main components of ATHENA are:

- High-Fidelity Dynamical Models
- Measurement Models
- State Estimation and Filtering techniques
- Uncertainty Propagation
- Path Planning techniques
- Planning & Scheduling Solver

ATHENA has been developed in MATLAB with a very modular oriented architecture. This allow the tool to be flexible, easy to upgrade with new features and easy to adapt to different types of problems. In Figure 1 the toolbox components are outlined. The Uncertainty propagation module will not be described in this paper and can be found in [1]. In fact ATHENA relies on the uncertainty quantification suite contained in SMART-UQ and invokes the desired technique when an uncertainty propagation analysis is required.

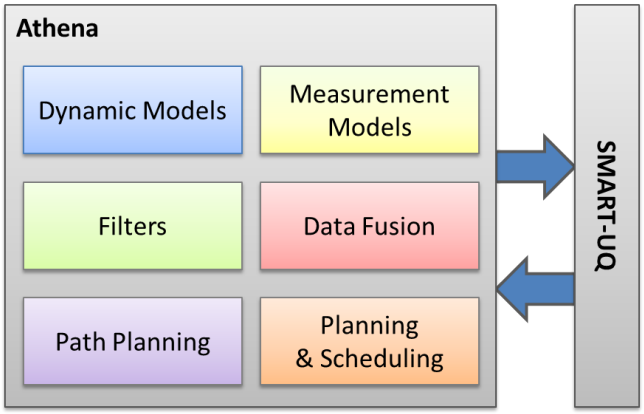

Fig. 1. ATHENA software architecture

2.1. Dynamic Models

The toolbox implements high fidelity models for both asteroids and Earth orbiting objects. The dynamic model includes third body effects, solar radiation pressure and the irregular gravity field of Earth, Moon and asteroids. In an inertial reference frame the dynamics is described in Cartesian coordinates:

$$\ddot{\mathbf{r}} = -\frac{\mu}{r^3}\mathbf{r} + \mathbf{a}_d \tag{1}$$

with μ the gravity constant, $\mathbf{r}$ the position vector and $\mathbf{a}_d$ collecting all accelerations, aside the one given by a central spherical gravity field. For proximity operations the dynamics is described in a Hill's reference frame:

$$\begin{aligned}\delta\ddot{\mathbf{r}}^h = &-\ddot{\mathbf{r}}_a^h - 2\dot{\theta}^h \times \delta\dot{\mathbf{r}}^h - \dot{\theta}^h \times \delta\mathbf{r}^h - \dot{\theta}^h \times \left(\dot{\theta}^h \times \delta\mathbf{r}^h\right) + \\ &- \frac{\mu_{Sun}}{r_{Sc}^3}\left(\delta\mathbf{r}^h + \mathbf{r}_a^h\right) + \nabla U_a + \frac{\mathbf{F}_{Sc}\left(\delta\mathbf{r}^h, \mathbf{r}_a^h\right)}{m_{Sc}}\end{aligned} \tag{2}$$

Equation (2) describes the motion of a spacecraft with position vector $\delta\mathbf{r}^h$ with respect to a celestial body with gravity constant μ_a. The Hill's reference frame is centred in the centre of mass of the celestial body. The celestial body has position vector $\mathbf{r}_a^h$ and angular velocity θ with respect to the Sun. The right hand side of the equation includes the Coriolis and centrifugal contributions, the gravitational attraction of the Sun, with gravity constant μ_{Sun}. The quantity ∇U_a represents the gravitational field of the celestial body, while the last term includes all non-gravitational accelerations like the solar radiation pressure.

The toolbox includes spherical harmonics gravity models, tetrahedral models from radar observations (see the example of Eros in Figure 2), and finite volume models. In the first case, the harmonic coefficients are from actual data or are calculated from the inertia matrix of a user-defined ellipsoid; in the last case, the gravity field is reconstructed from a point mass distribution.

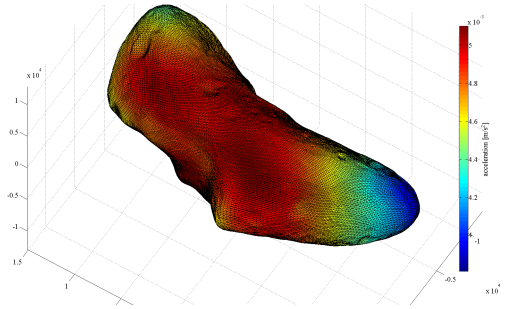

Fig. 2. Tetrahedron model of Eros from radar observations.

For the point masses model the expression of the gravitational potential is:

$$U_a = \sum_{i=1}^{N} \frac{\mu_{a,i}}{||\mathbf{r}_{Sc} - \mathbf{r}_i||} \tag{3}$$

where $\mu_{a,i}$ is the gravitational parameter of the i-th mass and $\mathbf{r}_i$ its position.

2.2. Measurement Models

The toolbox provides a number of sensor and measurement models. Some of the main sensor and measurement models are:

- **Camera Model** This model simulates a high resolution pin-hole camera (Figure 3). It provides the angular position of the target (elevation and azimuth angles), as well as optical flow measurement for tracked features.
- **LIDAR model** This model simulates the pulse laser which measures the travelling time of a pulse between the satellite and the target. It provides the distance from the spacecraft to a point on the targets surface.
- **Inter-Spacecraft Measurement Model** This model simulates the inter-spacecraft measurements. It provides the relative position, the relative attitude and the distance between two spacecraft.
- **Ground Station Measurement** This model simulates range (ρ) and range rate ($\dot{\rho}$) measurements with respect to a ground station. This set of measurements is the typical set used to estimate spacecraft trajectory from Earth [2]. This model includes the rotation of the Earth Effect.
- **Sun-Doppler Shift Model** This model simulates a resonance-scattering spectrometer instrument which measure the radial velocity of the spacecraft with respect to the Sun (Sun Doppler shift) [3]. The use of this kind of sensor is useful during the deep space navigation since could be used to integrate the relative and

angular measurement from the spacecraft formation during the period in which the formation is not visible from ground.

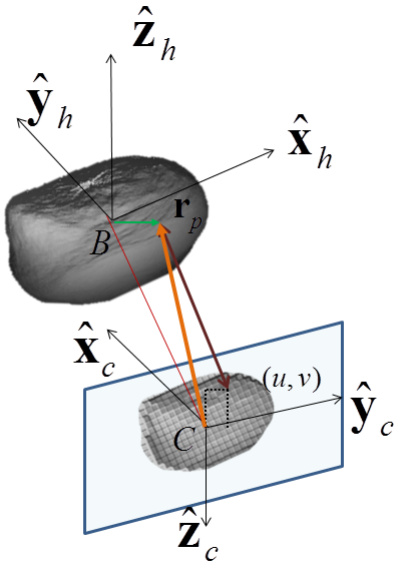

Fig. 3. Pin-Hole Camera model

More details about the sensors and measurement models can be found in [4, 5].

2.3. State Estimation and Filtering Techniques

ATHENA implements a number of linear and non-linear filtering techniques that can be coupled with the dynamic models to build different applications and study cases. The main filtering techniques included in the toolbox are:

- Kalman Filter (KF)
- Extented Kalman Filter (EKF)
- Uncented Kalman Filter (UKF)
- H_∞ Filter (UHF)
- Extended H_∞ Filter (EHF)
- High-order semi-Analytic Extended Kalman Filter (HAEKF), (with expansions up to the 3rd order).

All filters have been extended to allow datafusing sensor information from multiple platforms More details about the filtering techniques can be found at [5, 6].

2.4. Path Planning

ATHENA provides Guidance specially for close proximity operations, autonomous rendezvous and docking (RVD) by implementing a path planning algorithm that compute the optimal desired trajectory. As this is the reference trajectory that the chaser is following throughout the maneuver, two important key features are required: high performance and safety.

The first key feature is achieved by optimizing the approach phase of the trajectory trough an inverse optimization problem. The trajectory is firstly parametrized trough polynomials of a fixed, user-chosen degree. Some coefficients will be analytically computed to satisfy the initial and final constraints (position and velocity), while the free coefficients left will be used as optimization variables. The polynomial expressions function of these variables are derived and substituted into the controlled Tschauner Hempel equations [7] to compute the control. The free coefficients are then varied till a minimum manoeuvring ΔV is reached.

The second key feature, the safety, is guaranteed by means of a collision avoidance approach. Knowing the shape of the target it is possible to compute a 3D shape function which approximates the targets geometry and creates a safety region around the target called Keep Out Coating (Figure 4). It is then checked at each time instant if the trajectory is either inside or outside the target by substituting the chasers position components into the shape function and verifying the sign of the functions value. Clearly, as the target is rotating, the chasers positions components will be firstly expressed into the targets body frame by means of a simple frame rotation.

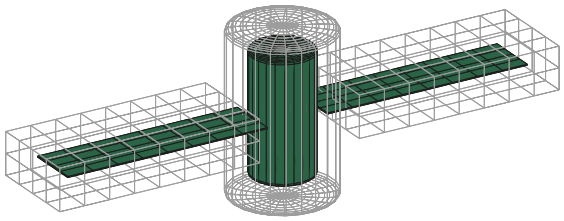

Fig. 4. Keep Out Coat Illustration

More details about the path planning algorithm can be found at [8].

2.5. Planning and Scheduling Solver

ATHENA provides planning and scheduling capabilities by integrating AIDMAP within the framework. AIDMAP (Automatic Incremental Decision Making And Planning) is a sin-

gle objective incremental decision making algorithm that allows to solve very complex combinatorial optimization problems such as tasks planning and scheduling.

One of the peculiarity of the AIDMAP is that the decision making problem is modelled using a tree-like topology, a decision tree where the nodes represent the possible decisions while links/edges represent the cost vector associated with the decisions. AIDMAP incrementally builds the decision tree from a database of elementary building blocks. These blocks represent a phase or leg of the mission. Using this approach eases the transcription of the problem into a tree-like topology. The resulting graph is then evaluated using a set of deterministic or probabilistic heuristics. The deterministic heuristics in AIDMAP are derived from classical Branch-and-Cut algorithms ([9, 10]) while the probabilistic heuristics are bio-inspired and mimic the evolution of the slime mould Physarum Polycephalum, a simple organism endowed by nature with a simple but powerful problem-solving heuristic [11, 12, 13, 14]. Unlike Branch-and-Cut that uses a set of deterministic branching and pruning heuristics, the Physarum algorithm uses probabilistic heuristics to decide to branch or prune a vein. To be more specific, branches are never really pruned but the probability of selecting them may fall to almost zero. A more detailed description about AIDMAP and the Physarum is given in [15, 11, 16].

Being able to solve planning and scheduling problems provides to ATHENA the capabilities to solve optimal sequence of tasks execution typically required to design close proximity operations or autonomous rendezvous and docking. In particular, ATHENA can generate optimal execution plans and control profiles to rendezvous with multiple targets or to dock multiple spacecraft with a single target.

3. APPLICATIONS

So far, ATHENA has been successfully used in four complex mission scenarios. In this section, the four mission scenarios are briefly presented in order to give a flavour of the capabilities and versatility of ATHENA together with the introduction of a work-in-progress project.

3.1. Navigating to the Moon in the Restricted Four Body Problem

ATHENA was originally developed to provide Orbit Determination (OD) and navigation analyses for the European Moon Orbiter (ESMO). ESMO was designed to reach the Moon by following a Weak Stability Boundary (WSB) transfer. The rich nonlinear dynamics of this type of transfers requires a particular navigation and control strategy to ensure capture into an uncontrolled relatively stable orbit at the Moon. Both uncertainty in the orbit determination process and in the control of the thrust vector were included in the navigation analysis. An Unscented Kalman Filter was used to do estimate position and velocity along the transfer trajectory starting from measurements coming from one or more ground stations. The interested reader can find more detailed information on this mission scenario in [6].

The navigation and control strategy was based on the definition of a capture corridor in the state space (Figure 5). The capture corridor is defined as the set of states that, at each time along the transfer, provides an uncontrolled weak capture at the Moon. The navigation and control strategy was ensuring that the spacecraft was within this corridor at any time during the transfer.

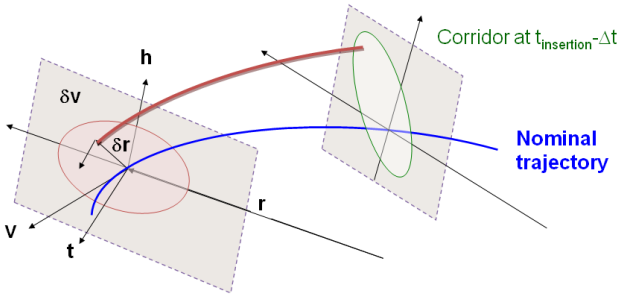

Fig. 5. Corridor Illustration

The observations and Trajectory Correction Manoeuvres (TCMs) were allocated so that the flow of possible trajectories coming from the errors in state estimation and manoeuvre execution was within the corridor. The convergence to the required set of states at injection was achieved by re-targeting the nominal solution and checking the inclusion in the corridor at different stages along the transfer. The aim of each TCM was to minimise the deviation from the nominal trajectory at certain points, called way-points. Figure 6 illustrates the navigation strategy along the WSB transfer. Two TCMs were allocated after each orbit determination to correct the trajectory up to the next way-point. The following constrained optimisation problem was solved to optimally define the magnitude of each pair of TCMs:

$$\begin{aligned} \underset{u \exists U}{\text{minimize}} \quad & \Delta v_{TCM_1} + \Delta v_{TCM_2} \\ \text{subject to} \quad & x(t_{wp}, u) - x_{Nominal}(t_{wp}) = 0 \end{aligned}$$

where $x_{Nominal}(t_{wp})$ is the nominal state of the spacecraft, and u is the control vector that must be optimized and contains the TCMs time of execution, direction and magnitude of the TCM.

Figures 7 show an example of targeting of the capture corridor after the last TCM. Yellow dot represent the desired capture corridor while black dots are the results of a Monte Carlo simulation of the controlled trajectory. As the figures show the inclusion in the capture corridor is guaranteed for the majority of the trajectory simulated during the Monte Carlo run.

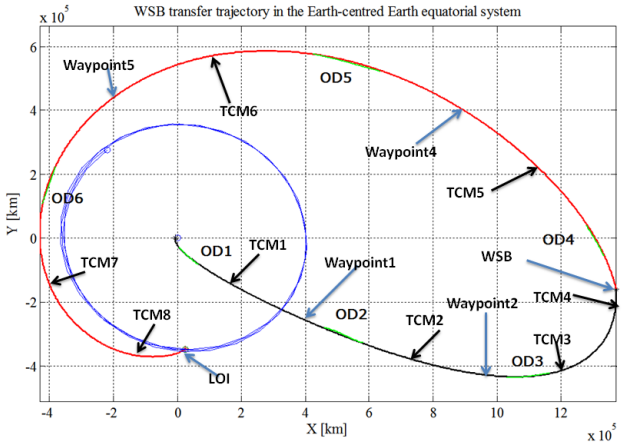

Fig. 6. Navigation Strategy along the WSB transfer

Three sequential filtering techniques were evaluated to establish which approach was the most suitable for the orbit determination and navigation strategy. These filters are: Extended Kalman Filter (EKF), Unscented Kalman Filter (UKF) and Kalman filter based on high order Taylor expansions.

Table 1. Elapsed CPU time for the filtering processes, using a 64-bit Linux CentOS 5.4, 2.93GHz Intel Xeon X5570, and absolute error for the estimated state.

	Elapsed CPU time [s]	Abs. Pos. Error [Km]	Abs. Vel. Error [mm/s]
EKF	20.52	6.657	26.48
UKF	47.02	0.765	4.94
HAEKF(2)	45.06	2.081	11.17
HAEKF(3)	1737.22	1.602	7.91

Table 1 shows the elapsed CPU time necessary to process all the measurements by the different filters. The most computational intensive filter is represented by the third order HAEKF (HAEKF s=3) itself, while the elapsed CPU time for the second order HAEKF (HAEKF s=2) and UKF is about 50 seconds. The EKF is the fastest method but it is still the least precise when compared to the other methods. The result of the comparison showed that all the filters are suitable, but best results are obtaining for third order HAEKF and for the UKF. However, the computational cost of the filters led to choose the UKF.

3.2. Collaborative Navigation and Control of a Formation in the Proximity of an Asteroid

This mission scenario considers the collaborative navigation and control of a formation of spacecraft around an asteroid. Each spacecraft in the formation is equipped with a sensor suite made of attitude sensors, a camera, a LIDAR and inter-satellite range and angular position measurements.

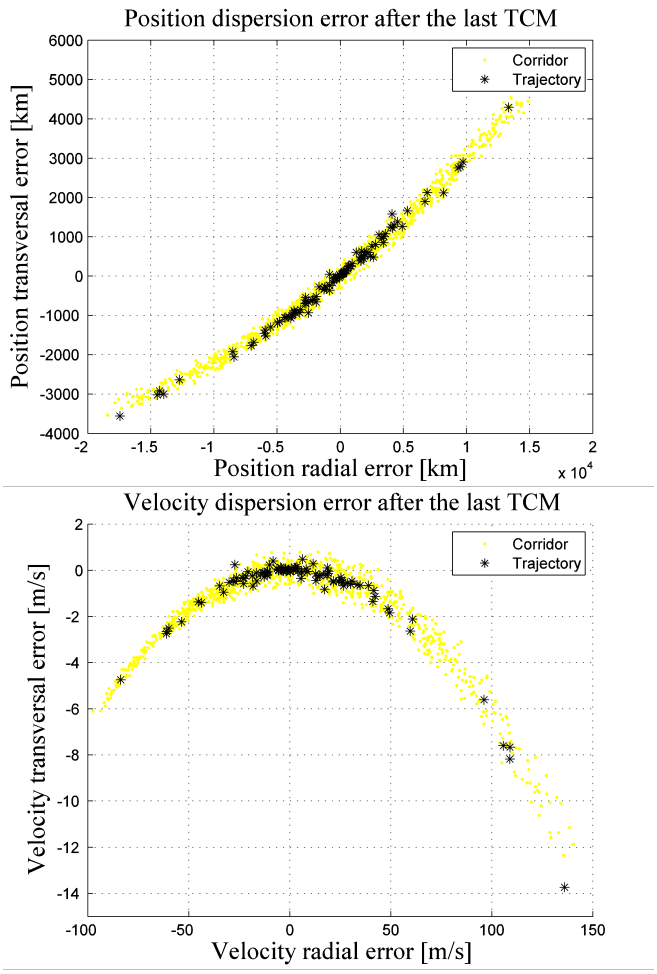

Fig. 7. Position and Velocity dispersion error for 100 runs after the last TCM in the r-t plane. The yellow points represent the corridor. 3% error on TCM.

A formation of 4-spacecraft is placed in the proximity of the Near Earth Asteroid (NEA) 99942 Apophis and expected to follow a set of predefined periodic orbits. Multiple measurements collected by the sensor suites on each spacecraft are exchanged, datafused and used to estimate the state of each spacecraft with respect to the asteroid. Inter-spacecraft links are proved to substantially improve accuracy and resilience in case of partial or total failure of some of the sensors. For the datafusion process four different filtering techniques were tested: EKF, UKF, EHF, UHF.

Table 2 reports the estimated initial states of the spacecraft in the Hill's reference frame of the asteroid. Figure 8 shows instead the reference periodic orbits each spacecraft has to follow. The initial mass of each spacecraft is 500 Kg, and the maximum cross section area is 20 m^2. A mean value of 1.2 for the reflectivity coefficient is assumed, with a uniformly

Table 2. Initial conditions for the spacecraft in the Hill reference frame of the asteroid.

	SC-1	SC-2	SC-3	SC-4
$x_h\ [Km]$	0.0323	0.0460	0.0323	0.0920
$y_h\ [Km]$	−0.500	−1.039	−0.503	−1.104
$z_h\ [Km]$	−0.774	−0.608	0.307	0.451
$\dot{x}_h\ [mm/s]$	0.193	0.051	0.259	0.009
$\dot{y}_h\ [mm/s]$	−4.480	−18.120	−4.533	−1.467
$\dot{z}_h\ [mm/s]$	−7.837	−6.350	−3.652	−4.942

distributed uncertainty of 20%. The GNC loop is closed using a Lyapunov controller.

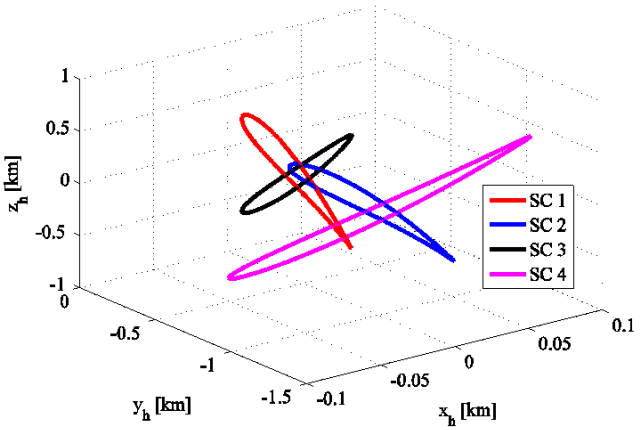

Fig. 8. Reference trajectories for the four spacecraft.

Different filters were considered to datafuse the measurements gathered by all the spacecraft. The selection of the optimal filter technique was based on the average RMSE and on the maximum steady state expected error (1-σ) after 1 day operations, reported in Table 3. As one can see the UHF presents superior performance compared to the other filters both in terms of estimated and controlled trajectory. The UHF is more accurate than the UKF with a RMS that is 25% lower in position and about 30% in velocity. When one considers the maximum expected errors, the UHF also presents the best results. One advantage of the unscented filters (UKF and UHF) is that they do not require the derivation and propagation of the Jacobian matrices. Although the computational cost is 20% greater than for the EHF, the UHF provided higher accuracy and robustness also in the estimation of the fully controlled trajectory.

The results for the error in position obtained for the controlled dynamics are showed in Figure 9 for the case in which the spacecraft share their measurements. The simulation spans 2 days with a time interval between measurements of 10 minutes. The test was repeated 100 times to assess the statistical relevance of the results. The use of a collaborative approach with shared measurements improves the accuracy already in the case all sensors are correctly working. Where the real advantage of a collaborative approach becomes evident is when some sensors malfunction. In the non-collaborative case the estimation error for each spacecraft is higher than in the collaborative case.

Table 3. Average RMSE comparison for different filters - SC-1

	UKF	EKF	EHF	UHF
CPU time [s]	1086	834	906	1140
RMSE position	24.03	24.30	18.18	17.78
(max 1-σ) [m]	(43.53)	(48.56)	(41.88)	(31.82)
RMSE velocity	2.27	2.41	1.88	1.59
(max 1-σ) [mm/s]	(2.71)	(2.97)	(2.60)	(2.03)
RMSE contr. pos.	27.27	27.89	20.50	20.39
(max 1-σ) [m]	(47.56)	(52.82)	(45.23)	(34.36)
RMSE contr. vel.	4.67	4.90	4.67	4.63
(max 1-σ) [mm/s]	(9.34)	(9.64)	(7.51)	(6.5)

Table 4. Test cases with failures.

Case	SC-1	SC-2	SC-3	SC-4
1	I	C,L/R,I	C,L/R,I	C,L/R,I
2	I	I	C,L/R,I	C,L/R,I
3	I	C,L/R,I	C,L/R,I	C,L/R*,I
4	I	I	C,L/R*,I	C,L/R*,I
5	I*	I*	C,L/R*,I	C,L/R*,I

C-camera, L/R-LIDAR, I-Inter-spacecraft
*degraded sensor

Table 4 reports the different cases used to assess the improvement of the estimation process in the case of failure or corrupted information. In the following, only the results for SC-3 and SC-4 are reported, because they present the worst and best results in terms of RMSE for all the cases. The trend for cases 1 to 4 is very similar to the collaborative case demonstrating that the inter-spacecraft link compensates for poor or incomplete direct measurements. In case 5, instead, spacecraft SC-3, experiences higher levels of error and the controller is not able to converge as in the other cases (Figure 10). Figure 11 shows that for SC-4 the oscillatory behaviour is less pronounced in cases from 1 to 4. In case 5, instead, SC-4 has a behaviour comparable to the one of SC-3, with maximum controlled position and velocity error respectively in the range 30-50 m and 3-6 mm/s (after the initial transient). More detailed information on this mission scenario can be found in [5].

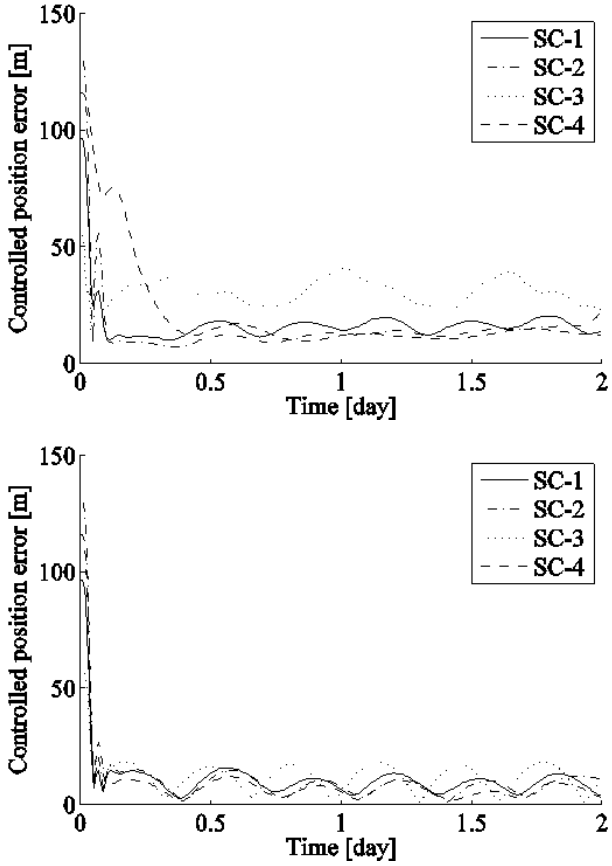

Fig. 9. Comparison between the error in position for the controlled dynamics without (top) and with (bottom) inter-spacecraft communication.

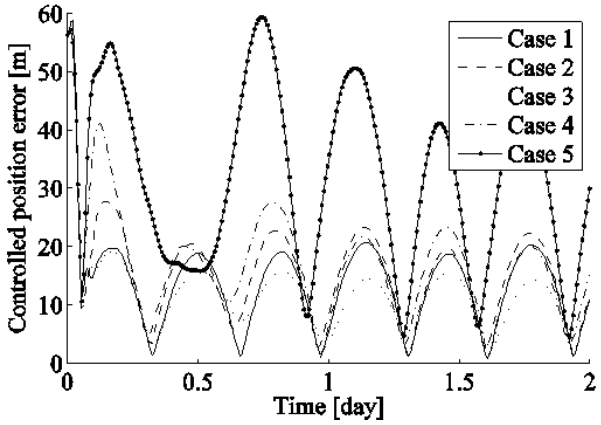

Fig. 10. Error in position for the controlled dynamics with inter-spacecraft communication for SC-3.

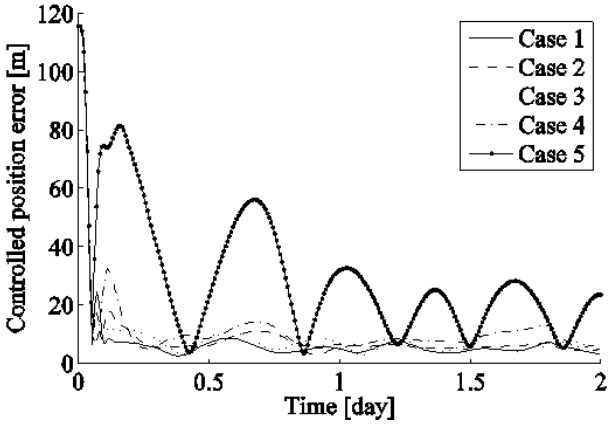

Fig. 11. Error in position for the controlled dynamics with inter-spacecraft communication for SC-4.

3.3. Asteroid ephemerides improvement via satellite measurements

In this mission scenario, an asteroid orbit determination method is proposed that combines asteroids line of sight measurements from multiple spacecraft and Sun Doppler shift sensor with spacecraft-to-ground tracking data. Different approach configurations are evaluated for a 2-spacecraft formation and it is shown that the integrated use of spacecraft-to-asteroid and ground-to-spacecraft measurements provides an effective way to improve the ephemerides of the asteroid. All the models and results presented here are extensively reported in [5].

In the following, it is assumed that two spacecraft will approach the asteroid at the same time when the asteroid is at perihelion. In such a situation, if the spacecraft formation travels from the Sun direction, given its visual magnitude of 19.7, the asteroid could be detected from a distance of about 2,000,000 km. We conservatively assumed that both spacecraft will concurrently start the acquisition of the target at 1,000,000 km from the asteroid.

The configuration of the approach and acquisition phase is depicted in Figure 12. The initial conditions are given with respect to the asteroids Hill reference frame in terms of distance, azimuth and elevation . Both spacecraft are placed at 1,000,000 km with an approach velocity of 100 m/s in magnitude directed along the spacecraft-to-asteroid vector. If the two spacecraft are separated by a small angle, the asteroid trajectory becomes poorly observable as it is not possible to accurately triangulate the position of the asteroid. Direct distance measurement from the asteroid to the spacecraft cannot be acquired using the LIDAR neither can the distance be derived from a single camera, unless complicated dogleg manoeuvres approach is adopted, because the shape of the asteroid might not be known in advance or the camera might not have a sufficiently high resolution. Therefore, the angular separation of the two spacecraft, seen from the asteroid, needs to be sufficiently high.

Table 5 reports the results for different configurations of

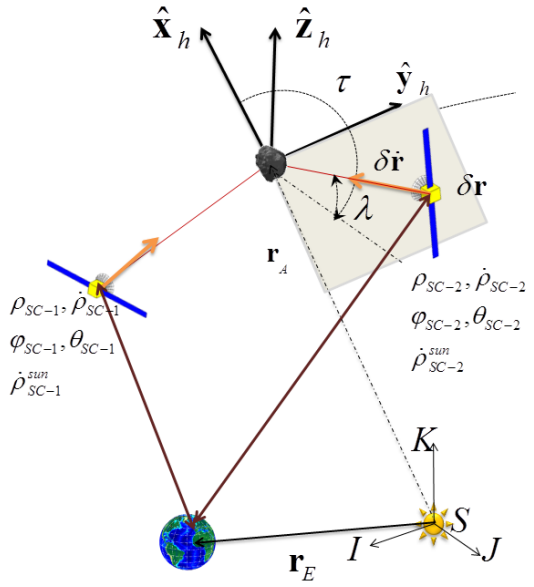

Fig. 12. Reference frames and notation for the improvement of the ephemerides of an asteroid.

τ and λ, each one simulated for 100 times. It is assumed that the measurement acquisition and state estimation processes run for 7 days. The first spacecraft was placed on the nominal orbit plane of the asteroid while the second spacecraft was given a maximum out of plane component equal to the asteroids initial dispersion in position that corresponds to a value of 3 degrees for λ. When the Doppler measurement is added, there is a general improvement of these estimates, especially for cases 1 and 7. However, for other configurations, the use of the Sun Doppler shift measurements does not lead to a noticeable improvement in the results. More detailed information on this mission scenario can be found in [5].

3.4. De-tumbling control of asteroids and space debris

This mission scenario presents an approach to control the rotational motion of an asteroid or a large piece of debris (satellite or rocket body) while a spacecraft is deflecting its trajectory through laser ablation. During the deflection, the proximity motion of the spacecraft is coupled with the orbital and rotational motion of the celestial body. The combination of the deflection acceleration, solar radiation pressure, gravity field and plume impingement will force the spacecraft to drift away from the celestial body. In turn, a variation of the motion of the spacecraft produces a change in the modulus and direction of the deflection action which modifies the rotational and orbital motion of the celestial body. An on-board state estimation and control algorithm in ATHENA simultaneously provides an optimal proximity control and a control of the rotational motion of the celestial body.

Table 5. Analysed configurations and final estimated error without and with Doppler shift.

	SC-1 τ [deg] λ [deg]	SC-2 τ [deg] λ [deg]	No Doppler Pos. Error [Km]	No Doppler Vel. Error [mm/s]	Doppler Pos. Error [Km]	Doppler Vel. Error [mm/s]
1	90 0	270 3	31.38	100.90	26.89	90.87
2	180 0	270 3	5.66	19.36	5.79	19.05
3	135 0	270 3	8.04	19.61	8.09	19.15
4	135 0	139 0	17.50	62.63	17.09	62.88
5	135 0	136 3	25.14	801.00	25.67	82.27
6	135 0	135.5 3	26.25	82.69	26.48	84.05
7	135 0	135.5 0.5	115.25	374.90	101.97	358.10

For the case of a 4m asteroid Figure 13 shows the estimation of the rotational states derived from optical flow measurement of some selected features.

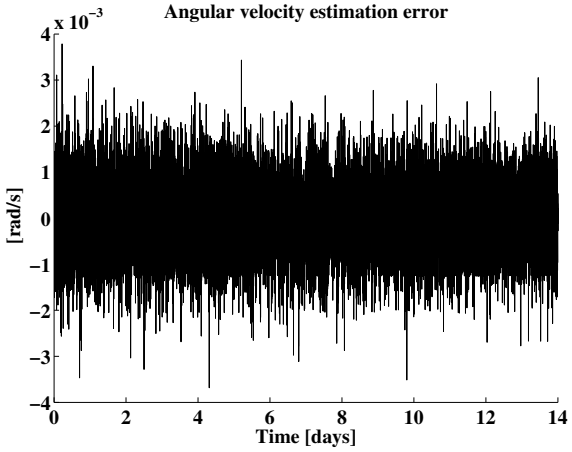

Fig. 13. Angular velocity estimation error

Figures 14 show, instead the accuracy to control the spacecraft to stay in a predefined control box at an average distance of 50m from the target. An interesting capability is the estimation of the acceleration induced by the laser ablation process on the asteroid. This acceleration cannot be directly measured and is instead derived as an unmodelled dynamic components by the filtering process.

Figure 15 shows the estimation versus the actual simulated acceleration.

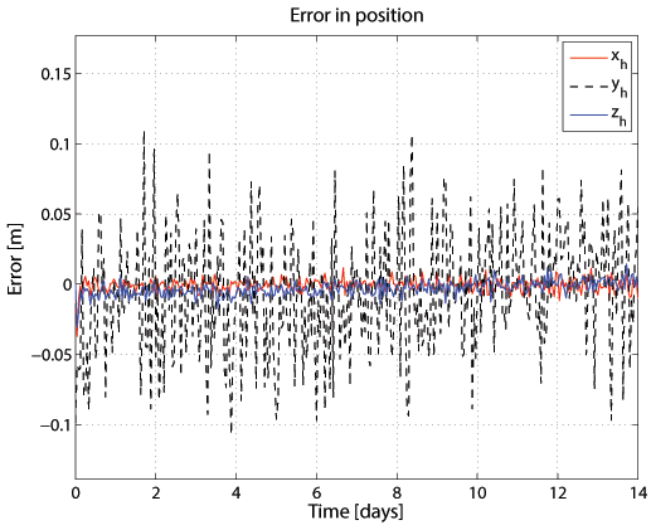

Fig. 14. Discrete Control - Actual controlled position (a) and velocity error (b).

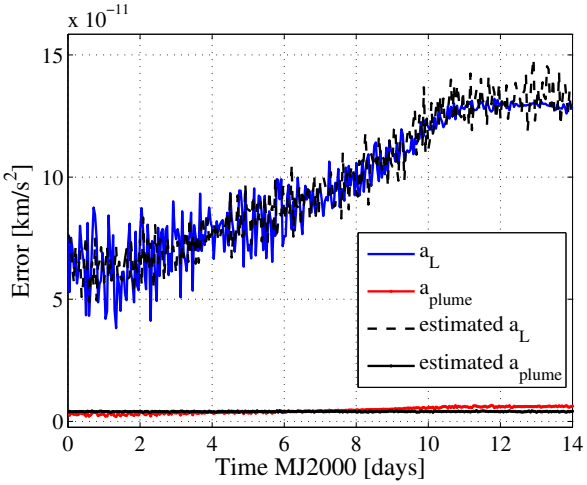

Fig. 15. Estimated acceleration from the laser and plume force vs. the actual acceleration. The dashed black line is the simulated acceleration induced by the ablation process, while the continuous black line is the simulated measurement from the impact sensor

For more details on the detumbling of asteroid please refer to [4].

3.5. Autonomous Collaborative On-Orbit Servicing

This study proposes an autonomy framework for autonomous On-Orbit Servicing (OOS) capable of planning and scheduling the execution of elementary pre-defined actions to fulfill complex OOS missions. The final aim of this study is to develop a framework for collaborative operations for a swarm of servicing spacecraft to perform multi docking and undocking operations in a coordinated manner.

This framework has been named as ACO^{2}SF (Autonomous Collaborative On-Orbit Servicing Framework). The two main components required by the framework are: i) a planning and scheduling solver and ii) a distributed GNC architecture, both required capabilities provided by ATHENA toolbox.

ACO^{2}SF is built on top of ATHENA and implements a cascade flow procedure architecture in which all the processes have been gathered in two consecutive layers: Decision Layer and Executive Layer. The Decision Layer is the first to be conducted in order to allocate the resources and to generate an optimal execution plan. In this layer, the most optimal path for each of the spacecraft is computed which includes collision avoidance with the target (possible, a non-cooperative tumbling target) and with the rest of the servicing spacecraft. This is essential to provide an optimal synchronized choreography for all of the agents that ensures safety through out all over the operation plan. Once all of the actions have been scheduled and assigned, the execution plan is carried out in the Executive Layer. All the servicing spacecraft conduct all the actions in a synchronized manner while keeping direct communication to react to any unforeseen event.

The ACO^{2}SF is responsible for:

- Allocate resources across the system
- Plan and schedule actions
- Execute the made decision
- Monitor the performance during the execution phase
- Provide contingency reactions to overcome any unforeseen event during the execution phase.

In order to provide safe autonomous docking, the path planning algorithm has to take into account the tumbling rate and the shape of the target to design the most optimal and safe path. Figure 16 shows an optimal path to dock with a triaxial tumbling target ($\omega_x = 0.02$, $\omega_y = 0.01$, $\omega_z = 0.01$) starting from a relative distance of 100m. This docking manoeuvring has an approximate cost of 8 m/s (ΔV) and a duration time of 96.6 min. Figure 16 shows the performance of the state estimation during the execution of the docking manoeuvring using the combination of a LIDAR and Camera models and the UKF.

However the aim of the framework is to provide an optimal execution plan for a collaborative swarm of servicing spacecraft. This aim is achieved by means of applying AIDMAP to solve the time-depended combinatorial problem. From a set of servicing spacecraft (resources), $S = \{C_1, C_2, C_3, \ldots, C_n\}$ and a set of tasks that have to be conducted in different docking points on the target , $D = \{DP_1, DP_2, DP_3, \ldots, DP_n\}$, AIDMAP computes the most optimal task sequence. Figure 18 illustrates a scenario where three servicing spacecraft are located in a control sphere of 100m of radius around the triaxial tumbling target,

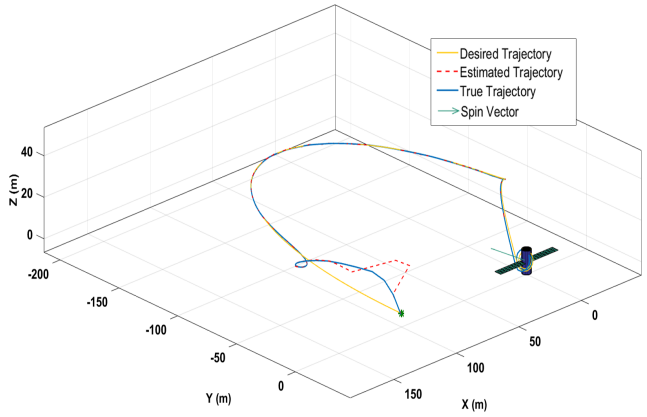

Fig. 16. Docking Path with a triaxial tumbling target

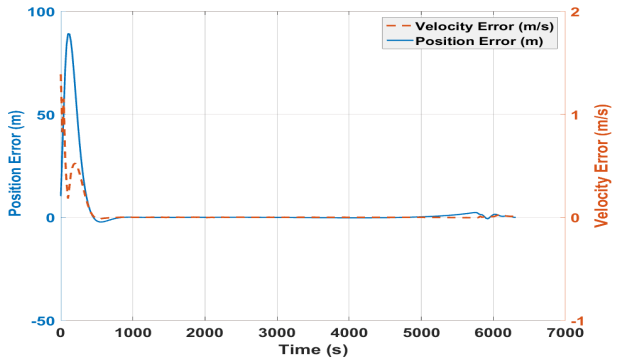

Fig. 17. Estimation Errors

described in the previous paragraph. Each of the servicing spacecraft have to carry out two operational tasks in any of the defined docking points. Every time one operational task has been concluded in any of the docking points, the servicing spacecraft has to return to the control sphere before to proceed with the following task. Table 6 reports the most optimal task sequence found for this example scenario characterized with a maximum total cost of $\Delta V = 113.2 m/s$.

Table 6. Collaborative Multi-Docking Solution

	Chaser	Docking Point	ΔV (m/s)
1st Docking	C_3	DP_3	16.8
& Undocking	C_1	DP_2	19.3
Phase	C_2	DP_1	16.7
2nd Docking	C_2	DP_2	16.4
& Undocking	C_1	DP_3	26.8
Phase	C_3	DP_1	17.3
		Total	**113.2**

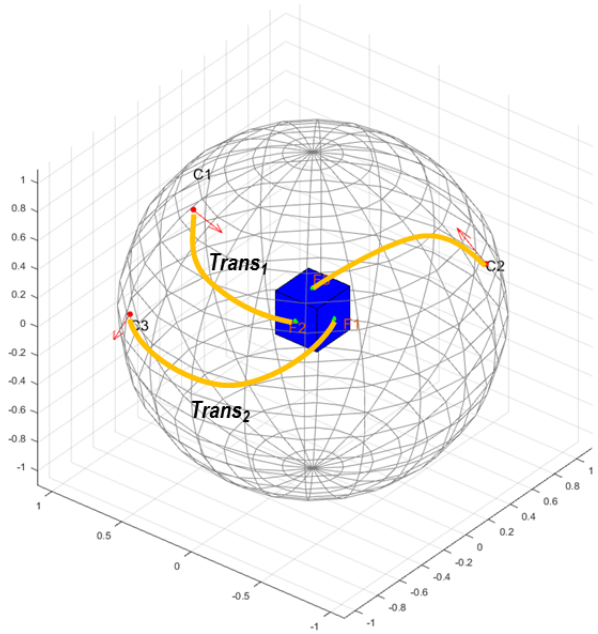

Fig. 18. Illustration of a collaborative multi-docking scenario

4. CONCLUSION

This paper presented the main features of ATHENA (Astrodynamics Toolbox for High-Fidelity Error and Navigation Analysis) toolbox developed at Aerospace Centre of Excellence of the University of Strathclyde to provide Guidance, Navigation and Control (GNC) solutions for a variety of complex mission scenarios.

It has been shown that the actual ATHENA toolbox is capable of dealing with the following applications: navigating to the Moon along low-energy transfers, autonomous navigation of a spacecraft formation in the proximity of an asteroid, asteroid ephemerides improvement via satellite measurements, asteroid rotation and orbit control via laser ablation and autonomous collaborative on-orbit servicing.

Results have shown that ATHENA can be applied successfully to a different variety of complex mission scenarios giving a very good performance. It has been shown the flexibility and the versatility of the toolbox.

5. FURTHER WORK

The team is currently working on developing and implementing new high precision techniques for the analysis of the motion of binary asteroid systems and the motion of spacecraft in their proximity. In addition, new sensor models are being implemented like FLASH LIDAR model together with new 3D shape reconstruction techniques to improve the pose and shape estimation of the target. Being able to generate docking path planning without having any a priori knowledge of

the shape of the target will improve the level of autonomy and safety of the servicing spacecraft to perform close proximity and RVD operations.

6. ACKNOWLEDGEMENTS

The authors would like to thank Renato Volpe, Master Student from Sapienza Universita di Roma for his contribution to the development of some part of the path planning algorithms.

7. REFERENCES

[1] A. Vasile M. Tardioli C. Ortega C., Riccardi, "Smart-uq: Uncertainty quantification toolbox for generalized intrusive and non intrusive polynomial algebra," in *ICATT*, Darmstadt, Germany, 2016.

[2] Catherine L Thornton and James S Border, *Radiometric tracking techniques for deep-space navigation*, John Wiley & Sons, 2003.

[3] Jo Ryeong Yim, John L Crassidis, and John L Junkins, "Autonomous orbit navigation of interplanetary spacecraft," in *AIAA/AAS Astrodynamics Specialist Conference, Denver, CO*, 2000, pp. 53–61.

[4] Massimo Vetrisano, Camilla Colombo, and Massimiliano Vasile, "Asteroid rotation and orbit control via laser ablation," *Advances in Space Research*, 2015.

[5] Massimo Vetrisano and Massimiliano Vasile, "Autonomous navigation of a spacecraft formation in the proximity of an asteroid," *Advances in Space Research*, 2015.

[6] Massimo Vetrisano, Willem Van der Weg, and Massimiliano Vasile, "Navigating to the moon along low-energy transfers," *Celestial Mechanics and Dynamical Astronomy*, vol. 114, no. 1-2, pp. 25–53, 2012.

[7] Mohamed Okasha and Brett Newman, "Guidance, navigation and control for satellite proximity operations using tschauner-hempel equations," *The Journal of the Astronautical Sciences*, vol. 60, no. 1, pp. 109–136, 2013.

[8] Renato Volpe, "Choreography on Elliptical Orbit," M.S. thesis, Sapienza Universita de Roma, 2016.

[9] M Jepsen, B Petersen, and S Spoorendonk, "A branch-and-cut algorithm for the elementary shortest path problem with a capacity constraint," *Department of Computer Science, . . . , ,* no. 08, 2008.

[10] Volker Schlecht, "Formulations and branch-and-cut algorithms for the generalized vehicle routing problem," *Investment Management and Financial Innovations*, vol. 5, no. 4, pp. 7–24, 2014.

[11] J. M. Romero Martin, L. Masi, M. Vasile, E. Minisci, R. Epenoy, V. Martinot, and J. Fontdecaba Baig, "Incremental planning of multi-gravity assist trajectories," in *65st International Astronautical Congress, IAC 2014*, 2014, pp. Paper–IAC.

[12] T. Nakagaki, H. Yamada, and Á. Tóth, "Intelligence: Maze-solving by an amoeboid organism," *Nature*, vol. 407, no. 6803, pp. 470–470, 2000.

[13] R. Kobayashi T. Saigusa T. Nakagaki A. Tero, K. Yumiki, "Flow-network adaptation in physarum amoebae," *Theory in Biosciences*, vol. 127, no. 2, pp. 98–94, 2008.

[14] L. Masi and M. Vasile, "A multidirectional physarum solver for the automated design of space trajectories," July 6-11, 2014.

[15] Romero Martin J. Vasile M. Di Carlo, M., "Camelot - computational-analytical multi-fidelity low-thrust optimisation toolbox," in *ICATT*, Darmstadt, Germany, 2016.

[16] Di Carlo M. Romero Martin, J. M. and M. Vasile, "Automatic planning and scheduling of active removal of non-operational satellites in low earth orbit," in *66st International Astronautical Congress, IAC 2015*, 2015, pp. Paper–IAC.